Journal of Nanobiotechnology

RESEARCH

Open Access

# Zinc-based radioenhancers to activate tumor radioimmunotherapy by PD-L1 and cGAS-STING pathway

Mengjiao Xu[1,2,3†], Chao Xu[3†], Yu Qiu[1,2†], Yushuo Feng[1,2†], Qianqian Shi[1,2], Yaqing Liu[1,2], Huaping Deng[1,2], Xiaoqian Ma[1,2], Nuo Lin[1,2], Qunying Shi[1,2], Zhiyang Shen[1,2], Shanshan Meng[1,2], Jiang Yang[4], Hongmin Chen[1,2,3*] and Fangqin Xue[3*]

## Abstract

Radiotherapy and immunotherapy have already become the primary form of treatment for non-small-cell lung cancer (NSCLC), but are limited by high radiotherapy dose and low immune response rate. Herein, a multi-pronged strategy using a radio-immuno-enhancer (ZnO–Au@m$SiO_2$) is developed by inducing tumor cells apoptosis and reprograming the immunosuppressive tumor microenvironment (TME). The radio-immuno-enhancer employed Au as a radiosensitizer, transition Zn ions as immune activators, which not only tremendously enhances the anti-proliferative activity of radiotherapy toward cancer cells, but also activates the immune response with multi-targets to let "exhausted" T cells "back to life" by triggering immunogenic cell death (ICD), immune checkpoint blockade (ICB) that target PD-1/PD-L1 and cGAS-STING under X-ray irradiation with a low dosage. The in vivo results demonstrate desirable antitumor and immunogenic effects of radio-immuno-enhancer-mediated immune activation by increasing the ratio of cytotoxic T cells (CTLs) and helper T cells. This work provides a feasible approach for future development of effective transition metal ion-activated radio-immunotherapeutic agents.

†Mengjiao Xu, Chao Xu, Yu Qiu and Yushuo Feng contributed equally to this work.

*Correspondence:
Hongmin Chen
hchen@xmu.edu.cn
Fangqin Xue
xfq9201125105@fjmu.edu.cn
Full list of author information is available at the end of the article

**Graphic Abstract**

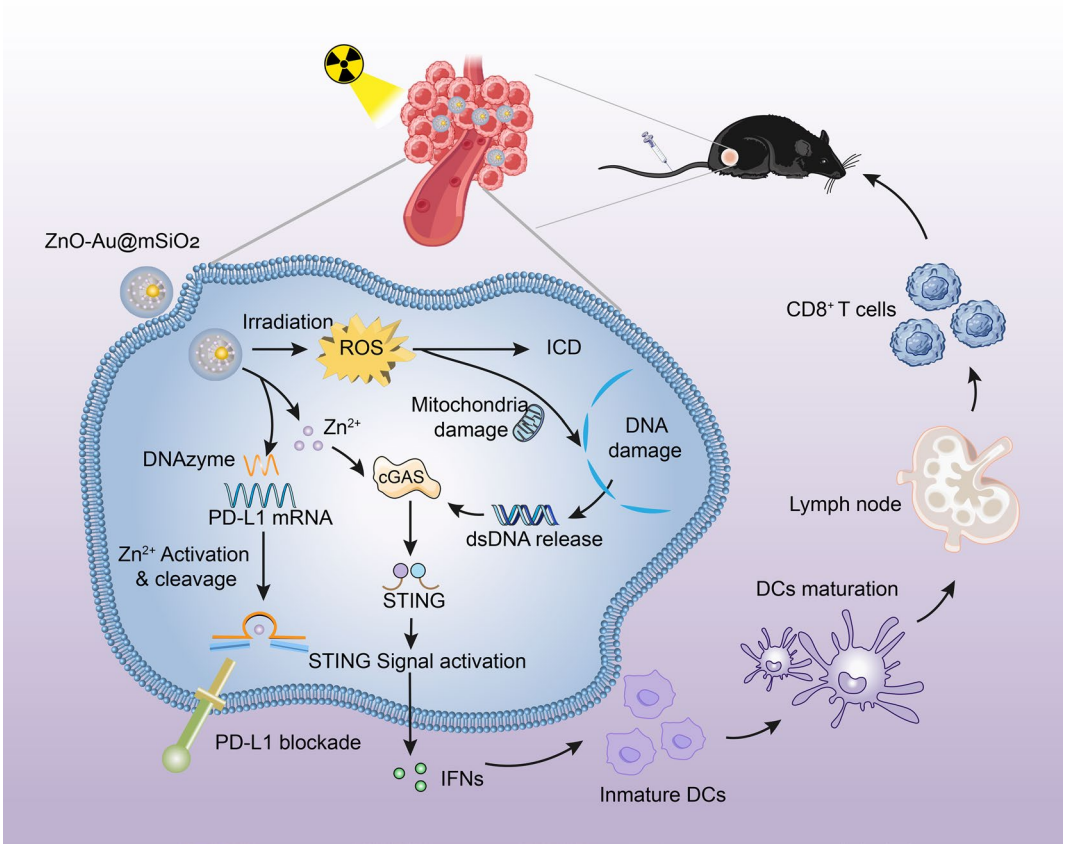


## Introduction

Non-small-cell lung cancer (NSCLC) is among the most deadly cancers, and has a poor prognosis [1, 2]. Radiation therapy (RT) is a widely used primary treatment modality for NSCLC that uses high-energy ionizing radiation with high dose to cause damage to tumor cells. As its therapeutic effect depends on the radiotherapy dose, it can cause acute lung injury and pulmonary fibrosis, affecting the prognosis [3–5]. Extensive studies have confirmed that immunotherapy is also an effective therapeutic strategy for NSCLC [1, 6–8]. The reversal of this impairment of immune system and the activation of the suppressed immune system could inhibit the growth of cancer cells or fully eliminate them. The scope of immunotherapy includes immunogenic cell death (ICD) response, immune checkpoint blockade (ICB) therapy, vaccines and adjuvants, which have provided a major breakthrough for the treatment of tumors [9–14]. Radiotherapy induces the occurrence of ICD, which could stimulate the release of tumor-associated antigens (TAAs) and the induction of damage-associated molecular patterns (DAMPs). These promote the activation and migration of dendritic cells (DCs), which then prime T cells for systemic anti-tumor immune responses [13, 15–17]. However, radiation-induced systemic immune responses are insufficient to meet clinical needs. There are few reports of radiotherapy-mediated immune activation [18–20], indicating there are huge challenges as well as enormous room for improvement.

The cyclic GMP-AMP synthase-stimulator of interferon genes (cGAS-STING) pathway, as a crucial part in innate immunity, is an important target for tumor therapy [21, 22]. Briefly, the cGAS/STING pathway can be activated by double-stranded DNA (dsDNA) to promote the secretion of type I interferons (IFNs), and induce the translocation of nuclear factor kappa-light-chain-enhancer of activated B cells (NF-κB) to the nucleus, which together induces the expression of inflammatory cytokines, thereby enhancing the specific killing effect on tumor cells. [23–26] As a vital component of living organisms, metal ions play an essential role in life

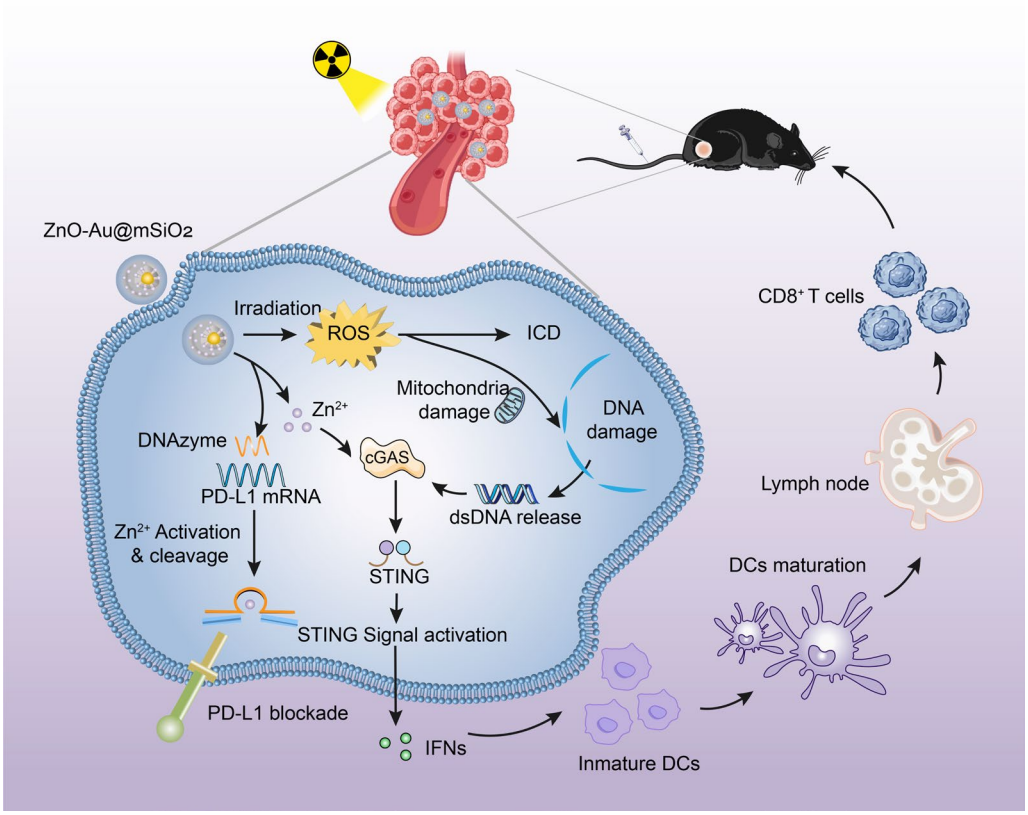


**Scheme 1** Scheme illustration of the ZnO–Au@mSiO$_2$ NPs for cancer immunotherapy. Mesoporous silica-encapsulated gold (Au@mSiO$_2$) nanoparticles were used as carriers for $Zn^{2+}$-dependent DNAzyme, which can act to degrade PD-L1, only after being activated by $Zn^{2+}$. ZnO, as a double activator for DNAzyme and cGAS-STING, was used as a "caretaker" to block off the pore of the SiO$_2$ for stability and safety (ZnO–Au@mSiO$_2$). The nanoparticles exposed to X-ray could enhance oxidative stress and immunogenic cell death (ICD), which would cause tumor cell apoptosis and activate the tumor immune response; the released $Zn^{2+}$ in acidic microenvironment activate the cGAS-STING signaling pathway for further amplifying the immune response, and activate DNAzyme for regulating PD-1/PD-L1 immunosuppression

processes, and they are ideally suited as signaling molecules for the immune system. Metal ions, such as Mn and Zn, have recently been developed as immunologic adjuvants to activate the cGAS-STING pathway [27–30]. Besides, nuclear damage and mitochondrial damage caused by radiotherapy have the potential to initiate the cGAS/STING pathway [31–33]. In several phase I/II trials, immune checkpoint inhibitors (ICIs) could effectively prevent recurrence and metastasis of NSCLC [34, 35]. Programmed death protein 1 (PD1) is a common immunosuppressive molecule on the surface of T cells. When it binds to its ligand, programmed cell death ligand 1 (PDL1), it participates in the immune evasion of tumors, leading to treatment failure. PD-1/PD-L1 inhibitors play an important role in the first- and second-line treatment of NSCLC, providing a new strategy and a key step for the treatment of NSCLC [36–38]. DNA enzymes could recognize specific mRNA sequences and cleave the target PD-L1 mRNA, thereby regulating the expression of PD-L1 in tumor cells. Designing responsively activated DNA enzymes can also improve the efficiency of targeted cutting of PD-L1 mRNA [39–42]. DNA enzymes with specificity for metal ions, such as Mn or Zn, are widely used in the diagnosis and treatment of tumors [43–45]. Immunotherapy has shown high clinical success rates, however, the efficacy of monotherapy is largely restrained by insufficient immune activation and the immunosuppressive tumor microenvironment (TME).

Herein, a synergistic strategy aiming to enhance the antitumor effects of radiotherapy and immunotherapy for NSCLC was designed (Scheme 1). Mesoporous silica-encapsulated gold (Au@mSiO$_2$) nanoparticles were designed as carriers of DNAzyme. ZnO was employed to block off the mesopore to stabilize the loaded DNAzyme, and ZnO was decomposed into free Zn ions to activate both DNAzyme and cGAS-STING. In vitro and in vivo investigations demonstrated that the radio-immuno-enhancers under X-ray irradiation could enhance oxidative stress and ICD, cause tumor cell apoptosis and activate the tumor immune response. This work provides

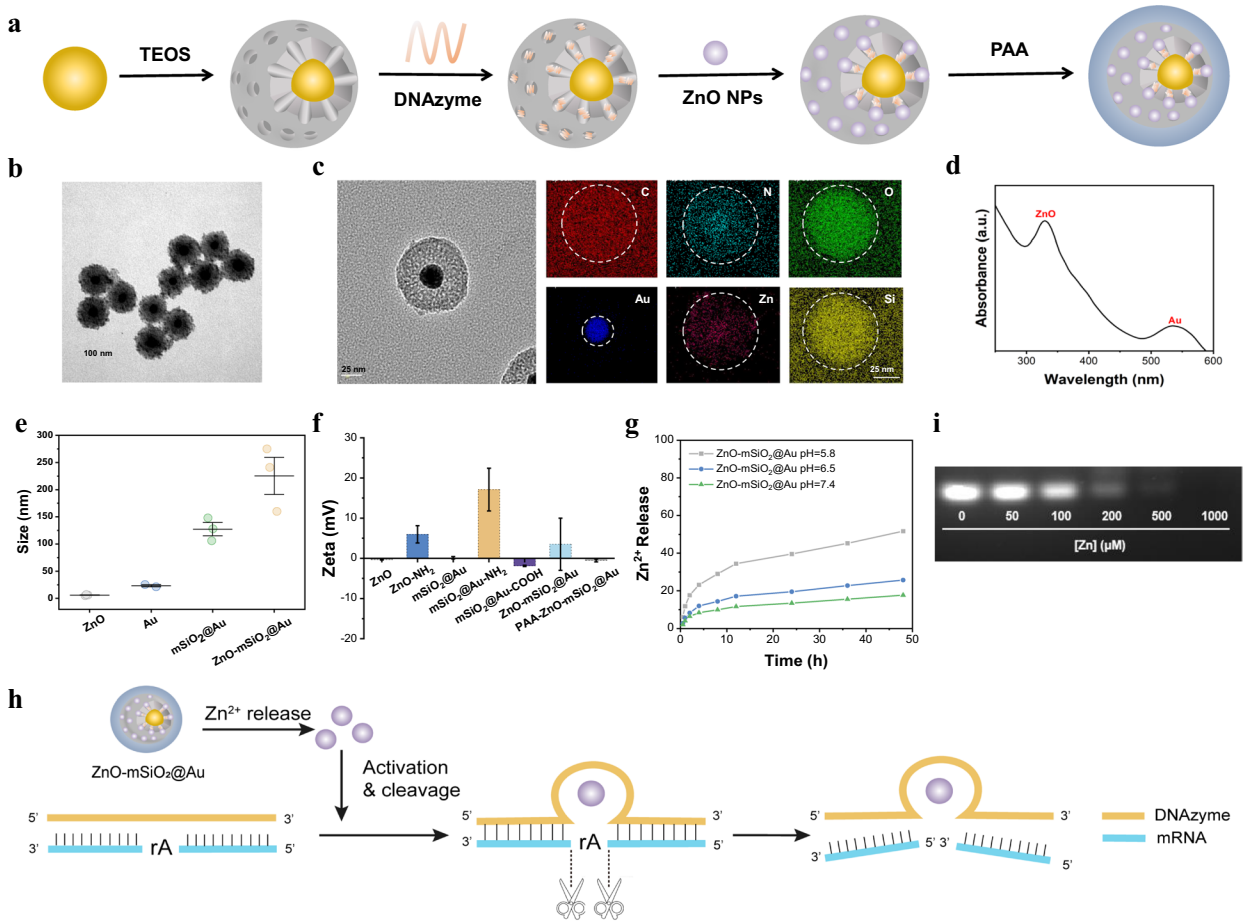


**Fig. 1** Preparation and characterization of ZnO–Au@mSiO$_2$. **a** Synthetic route of ZnO–Au@mSiO$_2$ nanocomposites. **b** TEM imaging of ZnO–Au@mSiO$_2$ nanoparticles. **c** STEM mapping analysis of ZnO–Au@mSiO$_2$. **d** UV–vis absorption spectra of ZnO–Au@mSiO$_2$. **e** The hydrodynamic diameter of structures. **f** Zeta potentials of structures. **g** Release of $Zn^{2+}$ from ZnO–Au@mSiO$_2$ under different conditions (pH 5.8, pH 6.5 and pH 7.4). **h** Schematic diagram of $Zn^{2+}$ release leading to activation of DNAzyme to cleavage target mRNA. **i** Gel electrophoresis images showing DNAzyme efficiency for substrate cleavage

a novel approach for enhancing NSCLC therapy via an effective metal ion-activated radio-immunotherapeutic strategy. The synergistic effect of the combined treatment modality of radiotherapy and ICI has been demonstrated in clinical trials. However, persistent immune activation may also lead to the development of pneumonia. In our design, $Zn^{2+}$ can achieve pH-responsive controlled release, thereby reducing the incidence of sustained immune activation. In addition, fluorescence imaging of ZnO–Au@mSiO$_2$ showed that there would be aggregation in the lung, which is a good condition for lung cancer treatment. This provides ideas for future clinical treatments, which could reduce the incidence of late toxic reactions to combination therapy while improving tumor control and overall survival [46, 47].

## Results

### Preparation and characterization of ZnO–Au@mSiO$_2$ nanoparticles

After DNAzymes were loaded in mesoporous silica (mSiO$_2$) with a gold core (Au @mSiO$_2$), ZnO clusters were employed to encapsulate the mesopores to block the release of DNAzymes and food additive polyacrylic acid (PAA) were then coated on surface to obtain biocompatible ZnO–Au@mSiO$_2$ (Figs. 1a–c, S1), which exhibited excellent stability in media (Figure S2). The characterizations of UV–vis absorption spectroscopy, DLS, zeta potential results and wide-angle X-ray diffraction (XRD) confirmed the successful synthesis of biocompatible ZnO–Au@mSiO$_2$ (Fig. 1d–f, S3).

The cumulative release kinetics of the $Zn^{2+}$ were detected in simulated solutions (pH 7.4 and pH 5.8). Analyzing results of free $Zn^{2+}$ in solutions indicated that 51.7% of $Zn^{2+}$ were released in acidic phosphate buffer

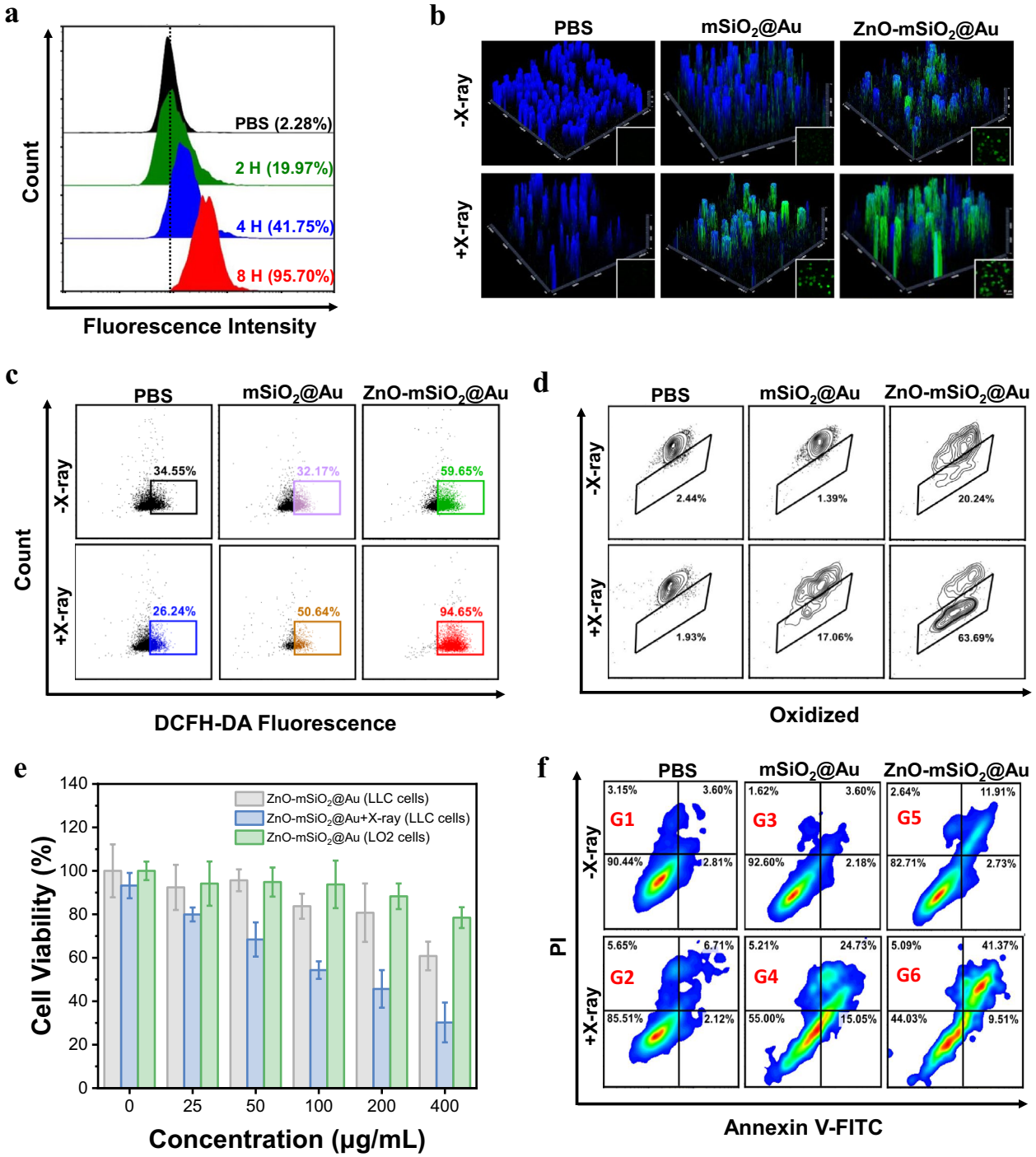


**Fig. 2** In vitro inhibition of tumor cell growth. **a** Cell uptake on LLC cells incubated with ZnO–Au@mSiO$_2$ analyzed by Flow cytometry at different time. **b** Intracellular ·OH generation detected by DCFH-DA probe (scale bar, 20 μm). **c** Flow cytometry data for DCFH-DA probe treated with different therapeutic groups. **d** Detection of lipid peroxidation by BODIPY-C11 staining in LLC cells incubated with different groups. **e** Cell viabilities of LLC cells and LO2 cells measured by MTT assays, after incubating with different concentration of ZnO–Au@mSiO$_2$ with or without X-ray. **f** Flow cytogram representing apoptosis assay based on Annexin V-FITC and propidium iodide staining of LLC cells after treatment with different therapeutic groups. Group 1: PBS, Group 2: PBS + X-ray, Group 3: Au@mSiO$_2$, Group 4: Au@mSiO$_2$ + X-ray, Group 5: ZnO–Au@mSiO$_2$u, Group 6: ZnO–Au@mSiO$_2$ + X-ray

saline (pH 5.8 PBS) within 48 h incubation, while only 17.7% of $Zn^{2+}$ were released in normal condition (pH 7.4 PBS) (Fig. 1g). The release of $Zn^{2+}$ activated DNAzyme to downregulate targeted mRNA (Figs. 1h, S4). Gel electrophoresis results revealed that the concentration-dependent of $Zn^{2+}$ enhanced the cleavage efficiency of DNAzyme (Fig. 1i). Only in the presence of both DNAzyme and $Zn^{2+}$, the targeted mRNA (PD-L1) bands were completely cleaved.

#### In vitro inhibition of tumor cell growth

It has been shown that nanoparticles exhibit size-dependent uptake by tumor cells. Nanoparticles with sizes ranging from 10 to 150 nm are considered to have the best EPR results. In addition, NPs > 30 nm in size tend to accumulate at the tumor site. Neutral and amphoteric ion-charged particles exhibit low plasma clearance, which leads to increased tumor uptake. NPs with negative zeta potential or neutral potential can achieve their long circulation in vivo. Particle size, shape and zeta potentials were also effective in the cytotoxicity of nanoparticles. Spherical nanoparticles are less toxic than fibrous nanoparticles, and neutral particles are less cytotoxic than charged nanoparticles [48–50]. The excellent biocompatibility of PAA coating ensured the efficient endocytosis of ZnO–Au@$mSiO_2$ by Lewis lung tumor cells (LLC) (Fig. 2a). X-ray irradiation and released $Zn^{2+}$ in tumor cells led to the generation of reactive oxygen species (ROS), and the combination of X-ray irradiation and released $Zn^{2+}$ generated more ROS (Fig. 2b). Quantitative analyses demonstrated that the ROS concentration generating with ZnO–Au@$mSiO_2$ plus X-ray treatment is approximately 2.7-fold, 3.6-fold and 1.6-fold amplified than that of PBS, X-ray irradiation, and ZnO–Au@$mSiO_2$ group, respectively (Fig. 2c). ROS generation induced intracellular lipid peroxidation of ZnO–Au@$mSiO_2$ plus X-ray irradiation was 26.1-fold higher than PBS, which was primarily attributed to more ROS production via both high-Z radiosensitization and the effect of $Zn^{2+}$ (Fig. 2d).

Obviously, these induced significant cytotoxicity on tumor cells. Under the concentration of 200 μg/mL (ZnO–Au@$mSiO_2$), the cell viability was 80.7 ± 13.4%. And the tumor cellular viability was sharply dropped to 45.7 ± 8.6% by the additional X-ray irradiation (Fig. 2e). Notably, normal human liver cells (LO2 cells) showed excellent tolerance to ZnO–Au@$mSiO_2$, manifesting its negligible cytotoxicity to normol cells (Fig. 2e). The apoptosis rate of LLC cells in ZnO–Au@$mSiO_2$ + X-ray group (41.4%) is much higher than that of PBS group (3.6%) (Figs. 2f, S5).

Radiation promotes the release of double-stranded DNA (dsDNA) from the nucleus and triggers the exposure of mitochondrial DNA (mtDNA) in the cytoplasm. Both of them are potent mediators for the initiation of the cGAS-STING pathway and subsequent transcription of type I interferon [33, 51–53]. The cGAS-STING pathway can synergize with the ROS-mediated ICD effect to trigger a more effective immune response (Fig. 3a) [54].

ROS has been reported to cause severe damage to cells resulting in reduced mitochondrial membrane potential (MMP) [55]. Compared to other groups, ZnO–Au@$mSiO_2$ + X-ray treated cells displayed distinctly increased green fluorescence and clearly declined red fluorescence using JC-1 assay, suggesting significant mitochondrial dysfunction (Fig. 3b, c). The fluorescence intensity of mitochondria labelled by Mito-tracker green decreased from 60.1 ± 2.4% (PBS) to 37.9 ± 3.9% (ZnO–Au@$mSiO_2$ + X-ray) (Fig. 3d). Moreover, the bio-TEM images of LLC cells treated with ZnO–Au@$mSiO_2$ plus X-ray demonstrated mitochondrial enlargement, swelling, and vacuolar degeneration of the mitochondrial cristae which drastically reduced its activity (Fig. 3e).

Apart from causing organelle damage such as mitochondrial damage, radiation also cause DNA damage in the nucleus. The extent of damage to the nucleus in the cell was evaluated by a variety of methods. Nuclear DNA damage was then assessed using immunofluorescence staining of γ-H2AX. The expression of γ-H2AX were significant higher in ZnO–Au@$mSiO_2$ plus X-ray group than in all Control groups, which was attributed to the

(See figure on next page.)

**Fig. 3** In vitro effects of mitochondrial damage, DNA damage, and proliferation ability. **a** Schematic diagram of the cGAS-STING signaling pathway induced by $Zn^{2+}$ and RT in tumor cells. **b** CLSM observation on the changes in the mitochondrial membrane potential of LLC cells after incubation with different treatment. The blue, red, and green colors indicate cell nucleus, and JC-1 aggregates and monomer, respectively (scale bar, 30 μm). **c** Flow cytometry analysis of mitochondrial membrane potentials using JC-1 after different treatments. **d** Active mitochondria were stained by mitochondrial probe Mito-Tracker Green after treatment with different groups and detected by FCM. **e** TEM images of mitochondrial morphological changes of LLC cells with different treatments (scale bar, local images: 1 μm, enlarged cell sections images: 200 nm). **f** The immunofluorescence images of γ-H2AX induced by DNA damage (scale bar, 10 μm). **g** The photographs of colony formation assay of LLC cells treated with PBS and different concentration of ZnO–Au@$mSiO_2$ under various radiation doses (0, 2, 4, 6 and 8 Gy). **h** Colony formation rate after treatment with ZnO–Au@$mSiO_2$. **i** Cell cycle analysis of LLC cells treated with PBS and ZnO–Au@$mSiO_2$ with or without X-ray and **j** analysis of flow cytometry

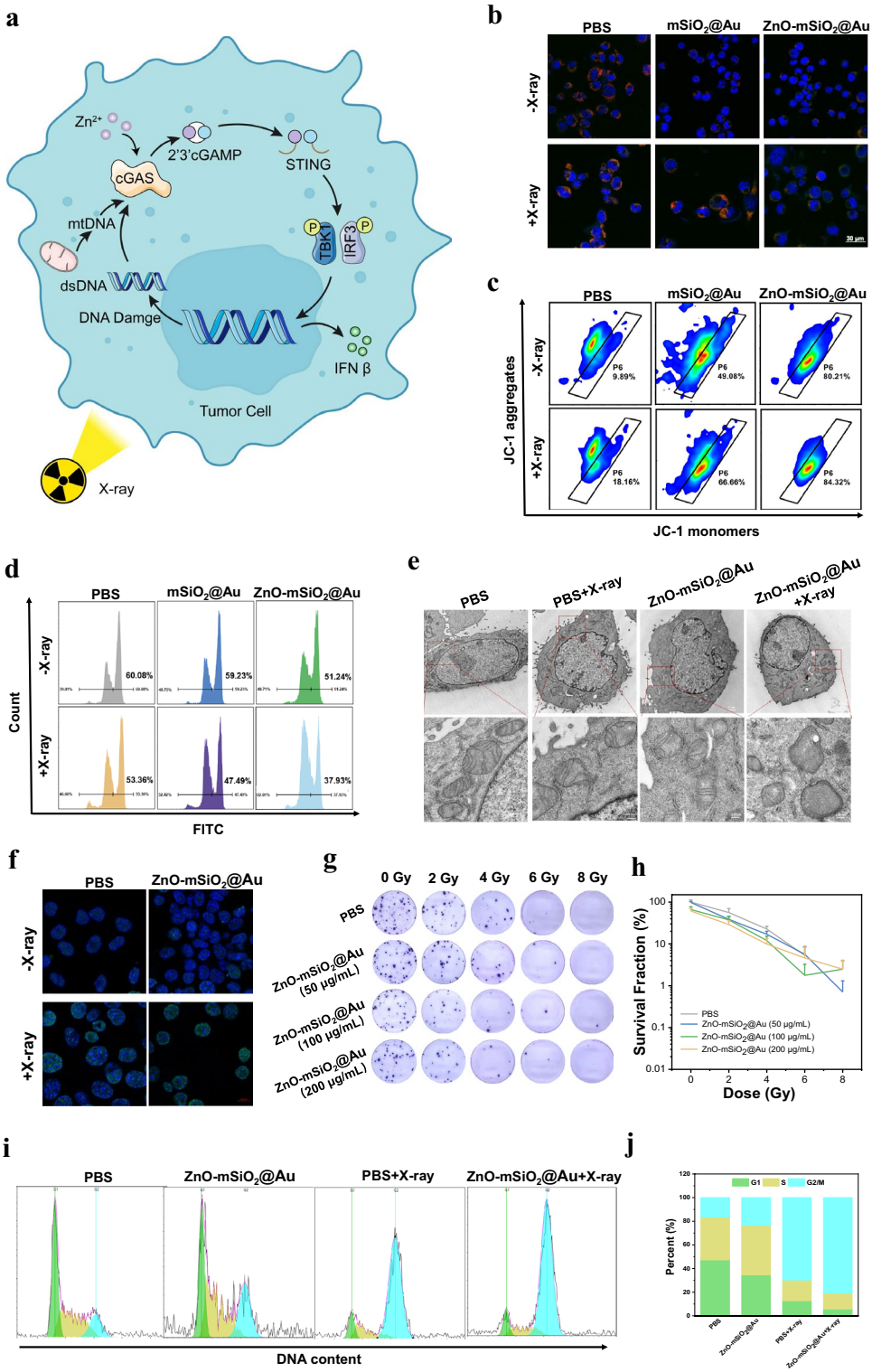


**Fig. 3** (See legend on previous page.)

combination effect of X-ray irradiation and $Zn^{2+}$ release (Fig. 3f). The cell cloning assay was performed to evaluate the impact on tumor cell proliferation for a long period of time. The results showed that ZnO–Au@$mSiO_2$-mediated RT was able to inhibit the long-term proliferative activity of tumor cells, which provided a reference for the

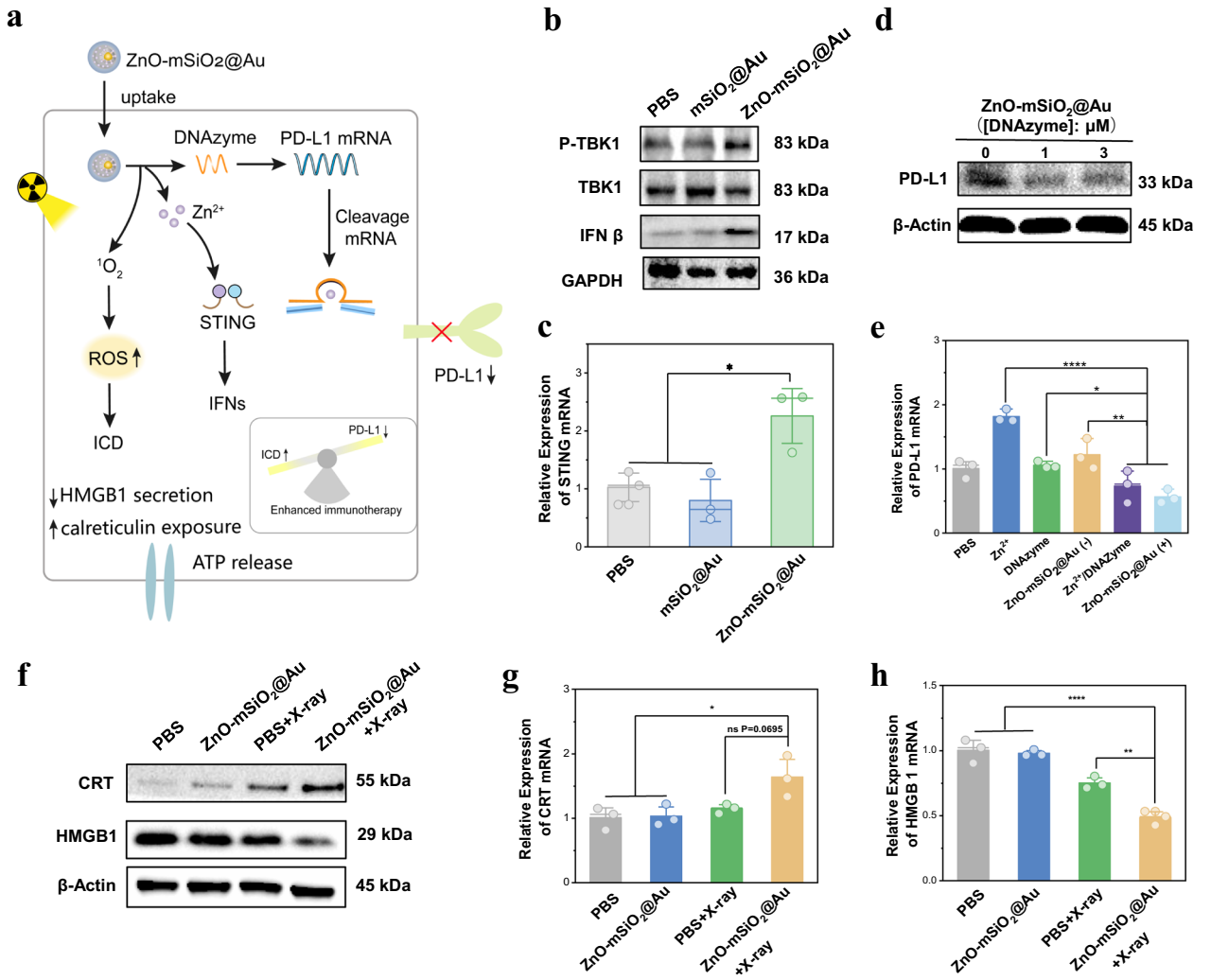


**Fig. 4** In vitro gene editing, RT-induced ICD and the cGAS-STING signal pathway-related genetic changes. **a** The role of ZnO–Au@mSiO$_2$ nanosystem after entering the cells. **b** Western blotting analysis for protein expression of cGAS-STING-associated proteins (IFN β, TBK1 and p-TBK1) in DC 2.4 cells. **c** qPCR assay measuring the STING mRNA in DC 2.4 cells (*p < 0.05). **d** Western blotting analysis for protein expression of PD-L1 in LLC cells. **e** qPCR assay measuring the PD-L1 mRNA in LLC cells, ZnO–Au@mSiO$_2$ (–) indicates that DNAzyme is not loaded, ZnO–Au@mSiO$_2$ (+) indicates that DNAzyme is loaded (*p < 0.05, **p < 0.01, ****p < 0.0001). **f** Western blotting analysis for protein expression of ICD-associated proteins (HMGB1 and CRT) in LLC cells. **g** qPCR assay measuring the CRT mRNA in LLC cells (*p < 0.05 and ns means no significant difference). **h** qPCR assay measuring the HMGB1 mRN A in LLC cells (**p < 0.01, ****p < 0.0001)

right choice of radiation dosage basis for subsequent animal experiments (Fig. 3g, h).

Cell cycle distribution of LLC cells after treating with ZnO–Au@mSiO$_2$ and X-ray was analyzed using PI staining. ZnO–Au@mSiO$_2$ caused the arrest of cells in the G2/M phase, convoyed by a decreased cell distribution in the G1 phase (Fig. 3i). The percentage of G2/M phase cells was obviously increased to 23.5% after treated with ZnO–Au@mSiO$_2$ compared with PBS group (16.4%) (Fig. 3j). Cells are sensitive to radioactivity, while the cells are in the G2 phase. As expected, ZnO–Au@mSiO$_2$ plus X-ray treatment caused a further larger G2/M phase arrest (80.6%) than only X-ray treatment (69.7%) (Fig. 3j). These results indicated that ZnO–Au@mSiO$_2$ + X-ray treatment might induce cell cycle arrest and prevent the cell clones from progressing through the cell cycle, delaying cell division.

As reported, Zinc finger structural domains in the binding region of cGAS and DNA enable the recognition of double-stranded DNA, while $Zn^{2+}$ enhances DNA-induced phase separation of cGAS and increases the catalytic activity of cGAS synthetase [21, 56, 57]. This

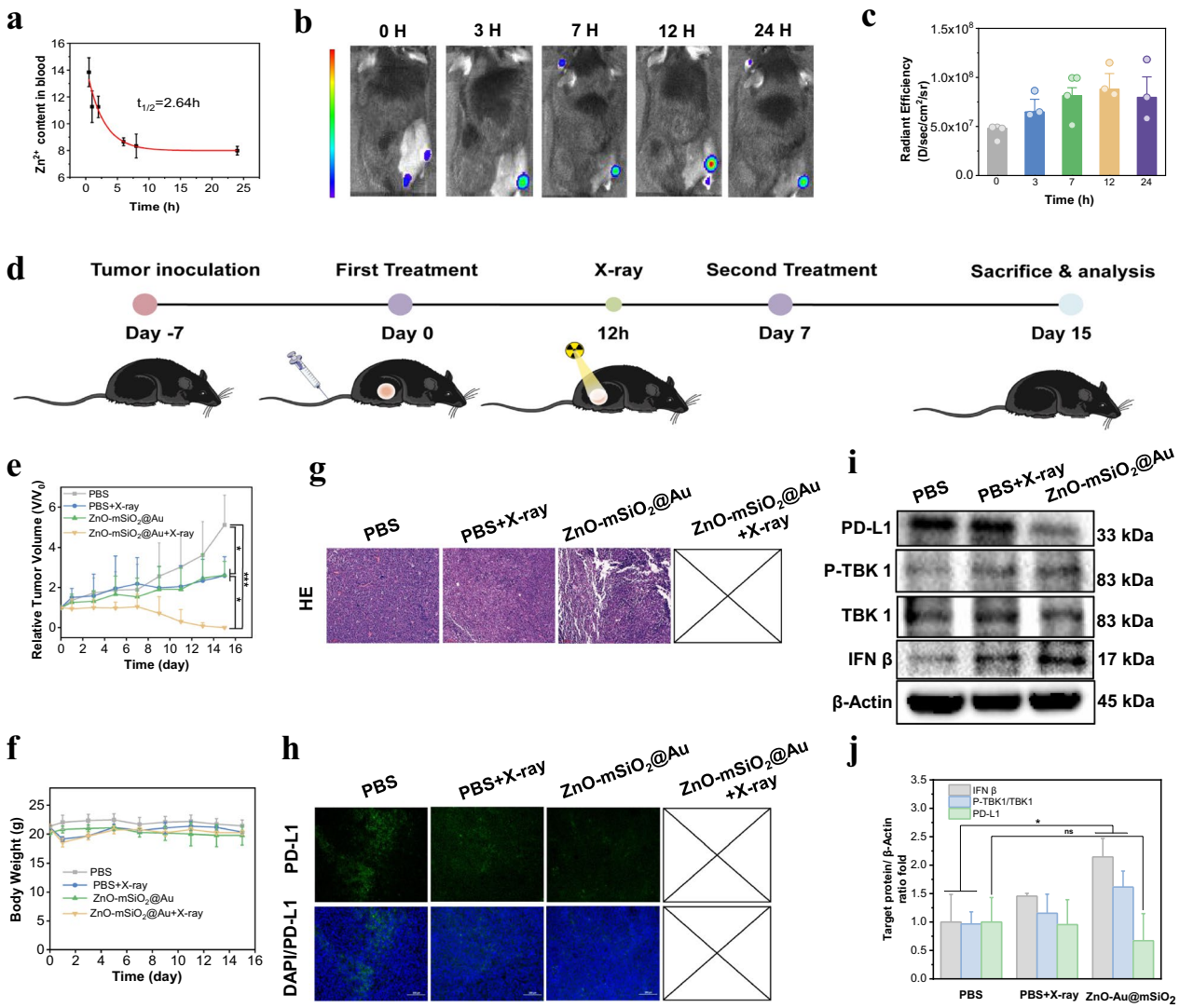


**Fig. 5** In vivo biodistribution and anti-tumor efficacy. **a** Pharmacokinetics of ZnO–Au@$mSiO_2$. **b** Fluorescence imaging of mice bearing LLC tumor at 0, 3, 7, 12, 24 h post-injection intravenously of ZnO–Au@$mSiO_2$-Cy5.5 (n = 3). **c** The corresponding fluorescence signals of subcutaneous tumors at 0, 3, 7, 12, 24 h post-injection intravenously of ZnO–Au@$mSiO_2$-Cy5.5. **d** Schematic illustration of the treatment process in mice bearing tumor. **e** The administration of the tumor volume changes in different treatment groups (n = 3) (*p < 0.05, ***p < 0.001). **f** The administration of mouse body weights in different treatment groups (n = 3). **g** Representative H&E staining images of tumor tissues collected from group 1, group 2 and group 3 (scale bar, 100 μm). **h** Immunofluorescence staining of PD-L1 in the tumor slices collected from group 1, group 2 and group 3 (scale bar, 100 μm). **i** Western blotting analysis for protein expression of PD-L1 and cGAS-STING-associated proteins (IFN β, TBK1 and p-TBK1) in tumor tissues. **j** The relative protein levels of survivin after different treatments

promotes the synthesis of second messengers (cGAMP) and the activation of the downstream TANK binding kinase 1 (TBK1) and interferon regulatory factor 3 (IRF3), leading to the production of type I interferon (IFNs), thus enhancing the specific killing effect (Fig. 4a). Therefore, the related down-regulation of proteins such as phosphorylated TBK1 (p-TBK1), TBK1 and IFN β was assessed using Western blotting after treating in DC 2.4 cells. The protein level of IFN β under ZnO–Au@$mSiO_2$ treatment was significantly elevated compare to the PBS group (Fig. 4b), which indicated that $Zn^{2+}$ ions had an activation effect on cGAS-STING signaling pathway. Meanwhile, similar change trend was observed in phospho-TBK 1 (p-TBK 1) protein expression level (Fig. 4b). To further evaluate the activation capacity of ZnO–Au@$mSiO_2$ for cGAS-STING signal pathway, quantitative polymerase chain reaction (qPCR) was used to detect the expression of related mRNA including STING, IFN β and

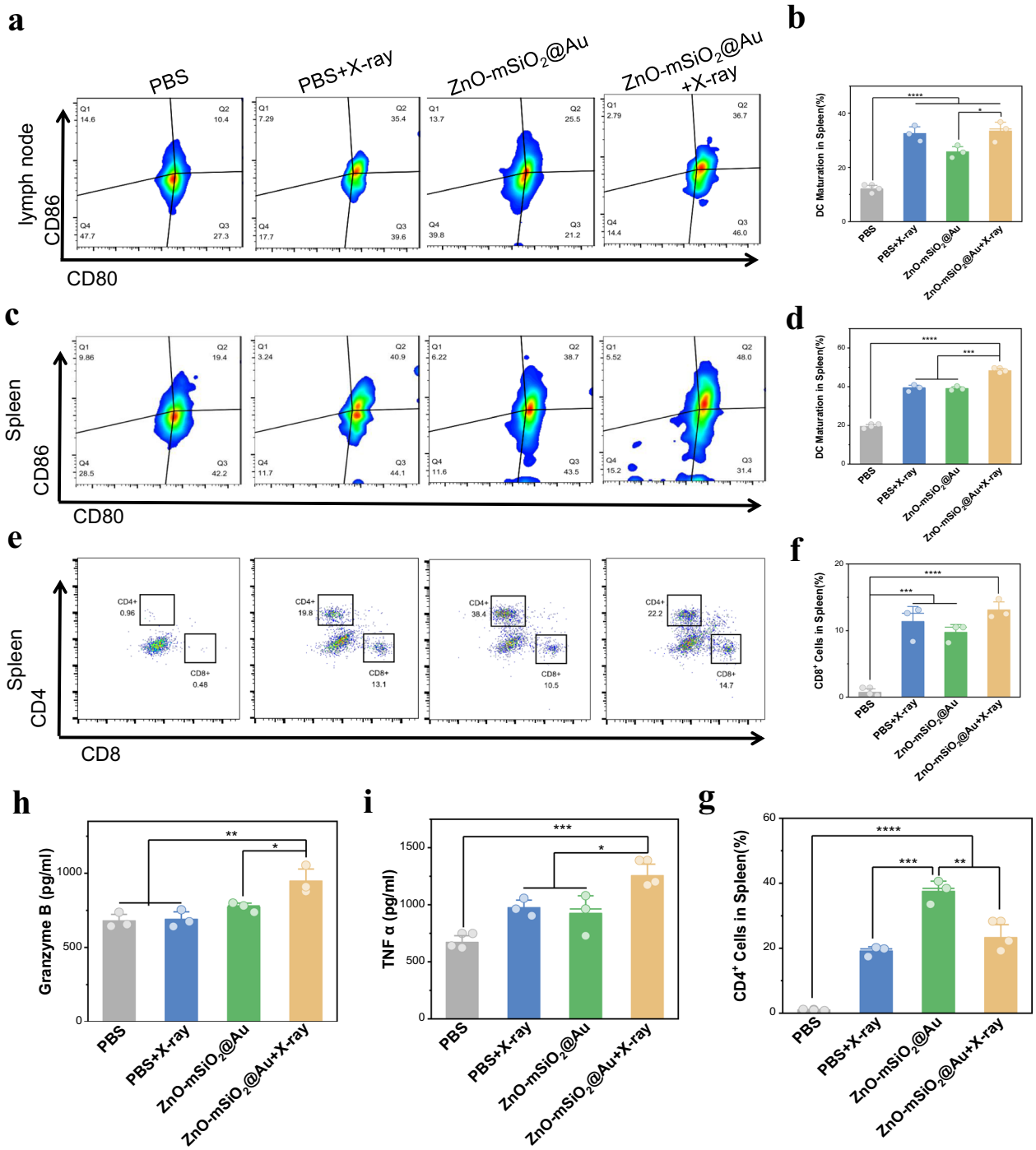


**Fig. 6** In vivo antitumor immune responses. **a** Representative flow cytometry plots and **b** corresponding quantification of DCs maturation in lymph node tissues (n = 3) (*p < 0.05, ****p < 0.0001). **c** Representative flow cytometry plots and **d** corresponding quantification of DCs maturation in spleen tissues (n = 3) (***p < 0.001, ****p < 0.0001). **e** Representative flow cytometry plots and **f**, **g** corresponding quantification of CTLs in spleen tissues (n = 3) (**p < 0.01, ***p < 0.001, ****p < 0.0001). **h** The expression levels of TNF-α and **i** Granzyme in serum analyzed by ELISA kit (*p < 0.05, **p < 0.01, ***p < 0.001)

TNF-α in DC 2.4 cells. According to the results obtained, ZnO–Au@$mSiO_2$ treatment significantly increased the expression of STING, IFN β and TNF-α in DC 2.4 cells (Figs. 4c, S6), which further validated that ZnO–Au@$mSiO_2$ could effectively activate the STING signal.

$Zn^{2+}$ acts as an immune adjuvant to activate the cGAS-STING signal pathway, meanwhile, it can also turn on the DNA enzyme to degrade PD-L1 mRNA. In our design, DNAzyme was employed to cleave PD-L1 mRNA, while $Zn^{2+}$ acted as a metal cofactor for DNAzyme activation. To confirm this self-activating gene regulation, we first evaluated the degradation effect by Western blotting. The PD-L1 protein expression level was downregulated in ZnO–Au@$mSiO_2$-treated cells (Fig. 4d). The qPCR further explored the PD-L1 mRNA expression, and the results were consistent (Fig. 4e). Importantly, neither $Zn^{2+}$ nor the DNAzyme alone could reduce the expression of PD-L1 (Fig. 4e). In brief, $Zn^{2+}$ as a cofactor, could upregulate the DNAzyme to cleave PD-L1 mRNA, achieving the aim of silencing the PD-L1 gene and regulating the tumor immunosuppressive microenvironment.

It has been reported that radiotherapy could induce significant ICD in tumor tissues [15]. In order to evaluate the ability of ZnO–Au@$mSiO_2$ to induce ICD in vitro, the release of ICD markers, such as calreticulin (CRT) and high mobility group box 1 (HMGB1) was examined. The results showed that ZnO–Au@$mSiO_2$ plus X-ray irradiation significantly promoted the expression of CRT and released HMGB1 compared with other experimental groups (Fig. 4f). Meanwhile, the qPCR obtained consistent results (Fig. 4g, h). All the above results indicated that ZnO–Au@$mSiO_2$ plus X-ray irradiation caused a higher degree of ICD than only ZnO–Au@$mSiO_2$ or X-ray irradiation treatment.

#### In vivo biodistribution and anti-tumor efficacy

Blood biochemistry and hematology analysis of healthy C57BL/6 mice after ZnO–Au@$mSiO_2$ administration showed that the relevant indicators were within the normal range (Figure S7, Table S1). The biodistribution of ZnO–Au@$mSiO_2$ was assessed in the subcutaneous LLC tumor model. The circulation of ZnO–Au@$mSiO_2$ in the bloodstream was found to follow the classical model (one-compartment model), and the calculated blood half-time was 2.6 ± 0.5 h, which are more beneficial for long-term tumor accumulation (Fig. 5a). The tumor accumulation of Cy5.5-labeled ZnO–Au@$mSiO_2$ NPs clearly indicated obvious fluorescence signals in tumor regions after 3 h post-injection, and reached at the maximum peak at 12 h post-injection (Figs. 5b, c, S8).

After validating biosafety and tumor accumulation on subcutaneous LLC tumor model in C57BL/6 mice, antitumor effects were investigated in vivo (Fig. 5d). When the tumor volume reached nearly 60 $mm^3$, mice were randomly divided into four groups (n = 3): PBS (Group 1), PBS + X-ray (Group 2), ZnO–Au@$mSiO_2$ (Group 3), ZnO–Au@$mSiO_2$ + X-ray (Group 4). The injection dose of ZnO–Au@$mSiO_2$ was 20 mg/kg. At 12 h post-injection, the tumors in Group 2 and 4 were irradiated with X-ray (4 Gy). On Day 7, the same procedure was repeated.

Compared to PBS, Group 2 and Group 3 showed moderate suppression of tumor growth (Figs. 5e, S9). Dramatically, complete tumor growth inhibition was observed in Group 4, i.e. ZnO–Au@$mSiO_2$ plus X-ray irradiation (Fig. 5e, yellow curve). In all treatments, no significant weight loss was found (Fig. 5f), indicating low side effects of the ZnO–Au@$mSiO_2$. Hematoxylin and eosin (H&E) staining of major organs (heart, liver, spleen, lungs, and kidneys) showed no obvious pathological changes, further implying the low systemic toxicity of ZnO–Au@$mSiO_2$ (Figure S10). Tumor growth in Group 4 was completely inhibited, leading to elimination, so only Groups 1–3 were compared. The results of H&E staining of tumors showed that the cell density, cell apoptosis and necrosis in the tumor tissue sections of the Group 2 and Group 3 were reduced, manifesting the effectiveness of ZnO–Au@$mSiO_2$ for treating subcutaneous tumors (Fig. 5g).

#### In vivo antitumor immune responses

Inspired by the superior therapeutical efficacy, we further explored the antitumor immune response. Tumor growth in Group 4 was completely inhibited, leading to elimination, and tumors from Groups 1–3 were used for protein extraction for Western blotting and immunofluorescence sections (Fig. 5h, i). The immunofluorescence images of PD-L1 showed that fluorescence signals of ZnO–Au@$mSiO_2$ were significantly reduced compared to other groups, demonstrating a decrease in PD-L1 expression (Fig. 5h). STING activation was also validated by Western blotting. The monotherapy group (radiotherapy group (X-ray) and ZnO–Au@$mSiO_2$ group) showed a remarkable increase of IFN β and phosphorylation of TBK1 (p-TBK1), indicating that radiotherapy and ZnO–Au@$mSiO_2$ could also contribute to the STING pathway activation (Fig. 5i). This has been attributed to the nuclear and mitochondrial damage induced by radiotherapy and the properties of Zn as an immune adjuvant.

We hypothesized that the ZnO–Au@$mSiO_2$-mediated immune activation mediated by ICD and STING pathway may promote the maturation of DCs. For the purpose, we examined mature DCs in lymph nodes and spleen. The Group 3 showed moderately promoted DC maturation, owning to the STING pathway activation, while Group 4 exhibited an apparent increase in the percentage of

activated DCs in lymph nodes (Fig. 6a, b). The results were consistent in the spleen (Fig. 6c, d). Mature DC cells contribute to subsequent activation of T cells, which are important immune cells for tumor inhibition. An obvious difference was found in the proportion of cytotoxic T cells (CTL, $CD3^+CD8^+$) among the Group 1 ($0.7 \pm 0.5\%$) and Group 3 ($9.7 \pm 1.1\%$) in the spleen (Fig. 6e, f). There was also a statistical difference in the results for T cells ($CD3^+CD4^+$) (Fig. 6g). We also detected the expression of TNF-α and Granzyme in serum treated with ZnO–Au@$mSiO_2$ + X-ray. The expression level of ZnO–Au@$mSiO_2$ + X-ray group increased, which enhanced the anti-tumor immune response in vivo through positive feedback, indicating the activation of body immunity (Fig. 6h, i). In summary, a robust anti-tumor immune response was observed in the reinforced immune microenvironment, suggesting the synergistic effects of $Zn^{2+}$-based cGAS-STING, PD-L1 inhibition and ICD targeted immunotherapy.

## Conclusion

In summary, this work presented a radio-immuno-enhancer that integrates radiotherapy and immune checkpoint therapy with immunoadjuvant therapy to improve the limitations of low immune response induced by mono-immunotherapy and enhance its anti-tumor efficacy. In vitro experiments demonstrated that the oxidative stress response triggered by radiotherapy increased the intracellular ROS content, induced damage, and resulted in the occurrence of ICD. The released $Zn^{2+}$ not only activated Zn-specific DNAzyme to cleave PD-L1 mRNA which can reduce immunosuppression and achieve immune checkpoint therapy, but also triggered the cGAS-STING signaling pathway that may enhance the expression of inflammatory cytokines and the activity of cytotoxic T cells. In vivo experiments demonstrated excellent anti-tumor activity with significant inhibition of tumor growth. This radio-immuno-enhancer can overcome the clinical side effects of high radiation dose of radiotherapy and low immune response of single-immunotherapy, reducing the incidence of sustained immune activation and providing a promising therapeutic strategy for anti-tumor immunotherapy of NSCLC through radioenhancers.

## Supplementary Information

The online version contains supplementary material available at https://doi.org/10.1186/s12951-024-02999-z.

Additional file 1.

**Acknowledgements**
Not applicable.

**Author contributions**
M. Xu, Y. Feng, H. Chen and F. Xue conceived and designed the research; M. Xu and Q. Shi performed the synthesis; Y. Feng, H. Deng and Q. Shi carried out the characterization experiments; X. Ma and N. Lin performed the cell experiment. M. Xu, Y. Feng and C. Xu performed the in vivo experiments; M. Xu, Y. Qiu, Z. Shen and S. Meng analyzed the data; M. Xu, Y. Feng, H. Chen and F. Xue co-wrote the paper. J. Yang, H. Chen and F. Xue provided academic leadership and guidance. All authors reviewed the manuscript.

**Funding**
The work was supported by the National Natural Science Foundation of China (82172007, 81771977), Joint Funds for the Innovation of Science and Technology Fujian province (2021Y9022), Joint Funds for the Innovation of Science and Technology Fujian province (2023Y9292), the Natural Science Foundation of Fujian Province (2023J011166, 2021J06007), Fujian provincial health technology project (2021QNA001), China foundation for youth entrepreneurship and employment, Open Funds of Guangdong Key Laboratory of Nasopharyngeal Carcinoma Diagnosis and Therapy (NPC2023-01), the Joint Funds for the Innovation of Science and Technology, Fujian province (2021Y9022), Key Clinical Specialty Discipline Construction Program of Fujian, China [(2022)884#]. All animal experiments were approved by the Animal Management and Ethics Committee of Xiamen University.

**Data availability**
No datasets were generated or analysed during the current study.

## Declarations

**Ethics approval and consent to participate**
All animal experiments were approved by the Animal Management and Ethics Committee of the Xiamen University.

**Consent for publication**
Not applicable.

**Competing interests**
The authors declare no competing interests.

**Author details**
[1]State Key Laboratory of Vaccines for Infectious Diseases, Center for Molecular Imaging and Translational Medicine, Xiang An Biomedicine Laboratory, School of Public Health, Xiamen University, Xiamen, China. [2]State Key Laboratory of Molecular Vaccinology and Molecular Diagnostics, National Innovation Platform for Industry-Education Intergration in Vaccine Research, Xiamen University, Xiamen, China. [3]Department of Gastrointestinal Surgery, Shengli Clinical Medical College of Fujian Medical University, Fujian Provincial Hospital, Fuzhou University Affiliated Provincial Hospital, Fuzhou, China. [4]State Key Laboratory of Oncology in South China, Guangdong Key Laboratory of Nasopharyngeal Carcinoma Diagnosis and Therapy, Guangdong Provincial Clinical Research Center for Cancer, Sun Yat-Sen University Cancer Center, Guangzhou, China.

Received: 18 April 2024 Accepted: 6 November 2024
Published online: 19 December 2024

**References**

1. Thai AA, Solomon BJ, Sequist LV, Gainor JF, Heist RS. Lung cancer. Lancet. 2021;398:535–54.
2. Passaro A, Brahmer J, Antonia S, Mok T, Peters S. Managing resistance to immune checkpoint inhibitors in lung cancer: treatment and novel strategies. J Clin Oncol. 2022;40:598–610.
3. Dasgupta Q, Jiang A, Wen AM, Mannix RJ, Man Y, Hall S, Javorsky E, Ingber DE. A human lung alveolus-on-a-chip model of acute radiation-induced lung injury. Nat Commun. 2023;14:6506–20.

4. Arroyo-Hernández M, Maldonado F, Lozano-Ruiz F, Muñoz-Montaño W, Nuñez-Baez M, Arrieta O. Radiation-induced lung injury: current evidence. BMC Pulm Med. 2021;21:9–21.
5. Käsmann L, Dietrich A, Staab-Weijnitz CA, Manapov F, Behr J, Rimner A, Jeremic B, Senan S, De Ruysscher D, Lauber K, Belka C. Radiation-induced lung toxicity-cellular and molecular mechanisms of pathogenesis, management, and literature review. Radiat Oncol. 2020;15:214–30.
6. Wang M, Herbst RS, Boshoff C. Toward personalized treatment approaches for non-small-cell lung cancer. Nat Med. 2021;27:1345–56.
7. Chaft JE, Rimner A, Weder W, Azzoli CG, Kris MG, Cascone T. Evolution of systemic therapy for stages I-III non-metastatic non-small-cell lung cancer. Nat Rev Clin Oncol. 2021;18:547–57.
8. Higgins KA, Puri S, Gray JE. Systemic and radiation therapy approaches for locally advanced non-small-cell lung cancer. J Clin Oncol. 2022;40:576–85.
9. Tay C, Tanaka A, Sakaguchi S. Tumor-infiltrating regulatory T cells as targets of cancer immunotherapy. Cancer Cell. 2023;41:450–65.
10. Topalian SL, Forde PM, Emens LA, Yarchoan M, Smith KN, Pardoll DM. Neoadjuvant immune checkpoint blockade: a window of opportunity to advance cancer immunotherapy. Cancer Cell. 2023;41:1551–66.
11. Chen Q, Chen M, Liu Z. Local biomaterials-assisted cancer immunotherapy to trigger systemic antitumor responses. Chem Soc Rev. 2019;48:5506–26.
12. Wang C, Ye Y, Hu Q, Bellotti A, Gu Z. Tailoring biomaterials for cancer immunotherapy: emerging trends and future outlook. Adv Mater. 2017;29: e1606036.
13. Huang Z, Wang Y, Yao D, Wu J, Hu Y, Yuan A. Nanoscale coordination polymers induce immunogenic cell death by amplifying radiation therapy mediated oxidative stress. Nat Commun. 2021;12:145–63.
14. Kim CG, Sang YB, Lee JH, Chon HJ. Combining cancer vaccines with immunotherapy: establishing a new immunological approach. Int J Mol Sci. 2021;22:8035–54.
15. Liu T, Pei P, Shen W, Hu L, Yang K. Radiation-induced immunogenic cell death for cancer radioimmunotherapy. Small Methods. 2023;7: e2201401.
16. Wang Y, Ding Y, Yao D, Dong H, Ji C, Wu J, Hu Y, Yuan A. Copper-based nanoscale coordination polymers augmented tumor radioimmunotherapy for immunogenic cell death induction and T-cell infiltration. Small. 2021;17: e2006231.
17. Wang Y, Chen J, Duan R, Gu R, Wang W, Wu J, Lian H, Hu Y, Yuan A. High-Z-sensitized radiotherapy synergizes with the intervention of the pentose phosphate pathway for in situ tumor vaccination. Adv Mater. 2022;34: e2109726.
18. Schaue D, Mcbride WH. Opportunities and challenges of radiotherapy for treating cancer. Nat Rev Clin Oncol. 2015;12:527–40.
19. Larson SM, Carrasquillo JA, Cheung NK, Press OW. Radioimmunotherapy of human tumours. Nat Rev Cancer. 2015;15:347–60.
20. Van Limbergen EJ, De Ruysscher DK, Olivo Pimentel V, Marcus D, Berbee M, Hoeben A, Rekers N, Theys J, Yaromina A, Dubois LJ, Lambin P. Combining radiotherapy with immunotherapy: the past, the present and the future. Br J Radiol. 2017;90:20170157.
21. Du M, Chen ZJ. DNA-induced liquid phase condensation of cGAS activates innate immune signaling. Science. 2018;361:704–9.
22. Hall J, Ralph EC, Shanker S, Wang H, Byrnes LJ, Horst R, Wong J, Brault A, Dumlao D, Smith JF, Dakin LA, Schmitt DC, Trujillo J, Vincent F, Griffor M, Aulabaugh AE. The catalytic mechanism of cyclic GMP–AMP synthase (cGAS) and implications for innate immunity and inhibition. Prot Sci. 2017;26:2367–80.
23. Chen Z, Li Z, Huang H, Shen G, Ren Y, Mao X, Wang L, Li Z, Wang W, Li G, Zhao B, Guo W, Hu Y. Cancer immunotherapy based on cell membrane-coated nanocomposites augmenting cGAS/STING activation by efferocytosis blockade. Small. 2023;19: e2302758.
24. Liang JL, Jin XK, Zhang SM, Huang QX, Ji P, Deng XC, Cheng SX, Chen WH, Zhang XZ. Specific activation of cGAS-STING pathway by nanotherapeutics-mediated ferroptosis evoked endogenous signaling for boosting systemic tumor immunotherapy. Sci Bull (Beijing). 2023;68:622–36.
25. Liao CY, Lei CQ, Shu HB. PCBP1 modulates the innate immune response by facilitating the binding of cGAS to DNA. Cell Mol Immunol. 2021;18:2334–43.
26. Hu MM, Shu HB. Mitochondrial DNA-triggered innate immune response: mechanisms and diseases. Cell Mol Immunol. 2023;20:1403–12.
27. Song W, Song SJ, Kuang J, Yang H, Yu T, Yang F, Wan T, Xu Y, Wei ST, Li MX, Xiong Y, Zhou Y, Qiu WX. Activating innate immunity by a STING signal amplifier for local and systemic immunotherapy. ACS Nano. 2022;16:15977–93.
28. Zheng Y, Chen J, Song XR, Chang MQ, Feng W, Huang H, Jia CX, Ding L, Chen Y, Wu R. Manganese-enriched photonic/catalytic nanomedicine augments synergistic anti-TNBC photothermal/nanocatalytic/immunotherapy via activating cGAS-STING pathway. Biomaterials. 2023;293: e121988.
29. Cao L, Tian H, Fang M, Xu Z, Tang D, Chen J, Yin J, Xiao H, Shang K, Han H, Li X. Activating cGAS-STING pathway with ROS-responsive nanoparticles delivering a hybrid prodrug for enhanced chemo-immunotherapy. Biomaterials. 2022;290: e121856.
30. Sun X, Zhang Y, Li J, Park KS, Han K, Zhou X, Xu Y, Nam J, Xu J, Shi X, Wei L, Lei YL, Moon JJ. Amplifying STING activation by cyclic dinucleotide-manganese particles for local and systemic cancer metalloimmunotherapy. Nat Nanotechnol. 2021;16:1260–70.
31. Zhou J, Zhuang Z, Li J, Feng Z. Significance of the cGAS-STING pathway in health and disease. Int J Mol Sci. 2023;24:13316–44.
32. West AP, Khoury-Hanold W, Staron M, Tal MC, Pineda CM, Lang SM, Bestwick M, Duguay BA, Raimundo N, Macduff DA, Kaech SM, Smiley JR, Means RE, Iwasaki A, Shadel GS. Mitochondrial DNA stress primes the antiviral innate immune response. Nature. 2015;520:553–7.
33. Storozynsky Q, Hitt MM. The impact of radiation-induced DNA damage on cGAS-STING-mediated immune responses to cancer. Int J Mol Sci. 2020;21:8877–99.
34. Provencio M, Nadal E, Insa A, García-Campelo MR, Casal-Rubio J, Dómine M, Majem M, Rodríguez-Abreu D, Martínez-Martí A, Carpeño JD, Cobo M. Neoadjuvant chemotherapy and nivolumab in resectable non-small-cell lung cancer (NADIM): an open-label, multicentre, single-arm, phase 2 trial. Lancet Oncol. 2020;21:1413–22.
35. Shu CA, Gainor JF, Awad MM, Chiuzan C, Grigg CM, Pabani A, Garofano RF, Stoopler MB, Cheng SK, White A, Lanuti M, D'ovidio F, Bacchetta M, Sonett JR, Saqi A, Rizvi NA. Neoadjuvant atezolizumab and chemotherapy in patients with resectable non-small-cell lung cancer: an open-label, multicentre, single-arm, phase 2 trial. Lancet Oncol. 2020;21:786–95.
36. Zhou L, Liang H, Ge Y, Ding W, Chen Q, Zhang T, Xiao L, Li Y, Dong J, He X, Xue F, Jiang L. Precisely targeted nano-controller of PD-L1 level for non-small cell lung cancer spinal metastasis immunotherapy. Adv Healthc Mater. 2022;11: e2200938.
37. Reck M, Remon J, Hellmann MD. First-line immunotherapy for non-small-cell lung cancer. J Clin Oncol. 2022;40:586–97.
38. Liu Y, Wang L, Song Q, Ali M, Crowe WN, Kucera GL, Hawkins GA, Soker S, Thomas KW, Miller LD, Lu Y, Bellinger CR, Zhang W, Habib AA, Petty WJ, Zhao D. Intrapleural nano-immunotherapy promotes innate and adaptive immune responses to enhance anti-PD-L1 therapy for malignant pleural effusion. Nat Nanotechnol. 2022;17:206–16.
39. Liu C, Chen Y, Zhao J, Wang Y, Shao Y, Gu Z, Li L, Zhao Y. Self-assembly of copper-DNAzyme nanohybrids for dual-catalytic tumor therapy. Angew Chem Int Ed Engl. 2021;60:14324–8.
40. Liu P, Shi X, Peng Y, Hu J, Ding J, Zhou W. Anti-PD-L1 DNAzyme loaded photothermal Mn(2+) /Fe(3+) hybrid metal-phenolic networks for cyclically amplified tumor ferroptosis-immunotherapy. Adv Healthc Mater. 2022;11: e2102315.
41. Wang H, Chen Y, Wang H, Liu X, Zhou X, Wang F. DNAzyme-loaded metal-organic frameworks (MOFs) for self-sufficient gene therapy. Angew Chem Int Ed Engl. 2019;58:7380–4.
42. Zhao X, Wang Y, Jiang W, Wang Q, Li J, Wen Z, Li A, Zhang K, Zhang Z, Shi J, Liu J. Herpesvirus-mimicking DNAzyme-loaded nanoparticles as a mitochondrial DNA stress inducer to activate innate immunity for tumor therapy. Adv Mater. 2022;34: e2204585.
43. Huang PJ, De Rochambeau D, Sleiman HF, Liu J. Target self-enhanced selectivity in metal-specific DNAzymes. Angew Chem Int Ed Engl. 2020;59:3573–7.
44. Wang X, Kim G, Chu JL, Song T, Yang Z, Guo W, Shao X, Oelze ML, Li KC, Lu Y. Noninvasive and spatiotemporal control of DNAzyme-based imaging of metal ions in vivo using high-intensity focused ultrasound. J Am Chem Soc. 2022;144:5812–9.

45. Qian RC, Zhou ZR, Guo W, Wu Y, Yang Z, Lu Y. Cell surface engineering using DNAzymes: metal ion mediated control of cell-cell interactions. J Am Chem Soc. 2021;143:5737–44.
46. Han C, Qiu J, Bai L, Liu T, Chen J, Wang H, Dang J. Pneumonitis risk after chemoradiotherapy with and without immunotherapy in patients with locally advanced non-small cell lung cancer: a systematic review and meta-analysis. Int J Radiat Oncol Biol Phys. 2024;119:1179–207.
47. Zhang A, Yang F, Gao L, Shi X, Yang J. Research progress on radiotherapy combined with immunotherapy for associated pneumonitis during treatment of non-small cell lung cancer. Cancer Manag Res. 2022;14:2469–83.
48. Xu M, Qi Y, Liu G, Song Y, Jiang X, Du B. Size-dependent in vivo transport of nanoparticles: implications for delivery, targeting, and clearance. ACS Nano. 2023;17:20825–49.
49. Öztürk K, Kaplan M, Çalış S. Effects of nanoparticle size, shape, and zeta potential on drug delivery. Int J Pharm. 2024;666: 124799.
50. Mohammad A, Piotr M. The toxicity of nanoparticles and their interaction with cells: an in vitro metabolomic perspective. Nanoscale Adv. 2023;5:2674–723.
51. Du SS, Chen GW, Yang P, Chen YX, Hu Y, Zhao QQ, Zhang Y, Liu R, Zheng DX, Zhou J, Fan J, Zeng ZC. Radiation therapy promotes hepatocellular carcinoma immune cloaking via PD-L1 upregulation induced by cGAS-STING activation. Int J Radiat Oncol Biol Phys. 2022;112:1243–55.
52. Motwani M, Pesiridis S, Fitzgerald KA. DNA sensing by the cGAS-STING pathway in health and disease. Nat Rev Genet. 2019;20:657–74.
53. Fang C, Mo F, Liu L, Du J, Luo M, Men K, Na F, Wang W, Yang H, Wei X. Oxidized mitochondrial DNA sensing by STING signaling promotes the antitumor effect of an irradiated immunogenic cancer cell vaccine. Cell Mol Immunol. 2021;18:2211–23.
54. Wang Y, Gong F, Han Z, Lei H, Zhou Y, Cheng S, Yang X, Wang T, Wang L, Yang N, Liu Z, Cheng L. Oxygen-deficient molybdenum oxide nanosensitizers for ultrasound-enhanced cancer metalloimmunotherapy. Angew Chem Int Ed Engl. 2023;62: e202215467.
55. Zhou M, Liang S, Liu D, Ma K, Yun K, Yao J, Peng Y, Hai L, Zhang Q, Wang Z. Manganese-enriched zinc peroxide functional nanoparticles for potentiating cancer immunotherapy. Nano Lett. 2023;23:10350–9.
56. Zhang L, Zhao J, Hu X, Wang C, Jia Y, Zhu C, Xie S, Lee J, Li F, Ling D. A peritumorally injected immunomodulating adjuvant elicits robust and safe metalloimmunotherapy against solid tumors. Adv Mater. 2022;34: e2206915.
57. Cen D, Ge Q, Xie C, Zheng Q, Guo J, Zhang Y, Wang Y, Li X, Gu Z, Cai X. ZnS@BSA nanoclusters potentiate efficacy of cancer immunotherapy. Adv Mater. 2021;33: e2104037.


## Publisher's Note